PROGRESSIVE STEP MAXIMUM POWER TRACKER FOR CASCADED INVERTER INDUCTION MOTOR DRIVE

SOURAV GHOSH, TAPAS KUMAR SAHA

This paper presents the idea of an isolated photovoltaic (PV) based cascaded two-level inverter (CTLI), driving squirrel cage induction motor (SCIM). The connected non-linear load approximately represents a centrifugal pump. The control system of this drive is based on a motor control system along with a progressive step perturb and observe (PSPnO) maximum power point tracking (MPPT) technique for the PV sources towards better utilization of the source. This PSPnO MPPT system intends to operate the SCIM so that the energy developed by PV is utilized entirely through variation of the dc-link voltages of the CTLI under both uncertain variances of non-linear load torque and unpredictable solar irradiance. This PSPnO MPPT algorithm has been engaged in the control scheme for generating reference dc-link voltage. This motor control system is designed to operate in a rotor-flux-oriented rotating reference frame. As for generating CTLI's switching pulses, the space vector pulse width modulation (SVPWM) technique has been used for its good dynamic response. The whole system is designed to be deployable on a low-computation device. The simulations conducted by Simulink and the results are furnished considering various operational conditions.

1. INTRODUCTION

A non-linear source like the photo-voltaic (PV) cell requires a good mathematical expression like "single-diode" and "double-diode" models. The study of comparisons of different aspects of the model [1–3] is enough to understand that, for this work, a single-diode model of PV cells should serve the purpose.

Maximum power point tracking (MPPT) traces the operational intersection of voltage and current at which maximum power yield is ensured. A comprehensive assessment of various MPPT techniques has been conducted by the authors of [4–6], detailing their advantages and limitations. The analysis reveals that the fixed step perturbs and observe (FSPnO) MPPT approach demands minimal computational resources; however, it may be vulnerable as it has slow response and convergence, output oscillation, and is problematic in tracking local maxima during partial shading conditions (PSC), even with optimal parameter settings. Alternative techniques proposed in [7,8] demonstrate the capability to address these issues, though unsuitable for application on constrained computational power devices.

The variable step MPPT comes into the picture to balance simplicity and efficiency. The authors of [9] have developed a variable step of specific sizes MPPT that deals with generation from wind energy. In the paper [10], the authors employed a more refined version of the variable step MPPT, where they designed a PID controller to determine the current state's step size. In [11], the duty ratio of a 2-stage converter is changed by variable step size depending on both slopes of the power vs voltage curve. At the same time, artificial intelligence methods for step size determination have also been implemented [12,13] to resolve the issue. However, all of them require extensive computation power for real-time computation.

A method of evading PSC is reconfiguring the PV panel arrangement to produce higher voltage to meet the system requirements [14,15] utilizing a switching matrix and incremental conductance MPPT algorithm. However, if low voltage is used on the dc-bus along with a particular arrangement of PV panels, the PSC problem can be eliminated even with fixed panel arrangements. Another approach to resolving the PSC issue is deploying the P&O and Beta method [29]. The PSC issue of a lower output condition of the PV has been successfully addressed in the present work. This work also addresses issues related to slower tracking, all while operating seamlessly on a low computational power device that is deployable for practical application.
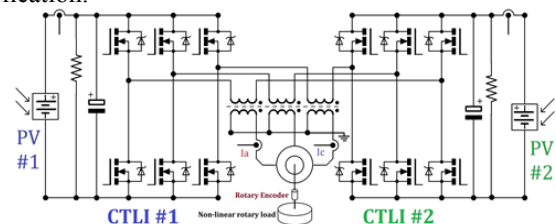

Fig. 1 – Power circuit of the proposed system.

A PV inverter system is a power circuit comprising two stages [16–20]. The primary stage maintains the dc-bus voltage/current at a fixed point in the system requirements. The subsequent stage converts the dc voltage into the specified ac voltage by switching arrangements. Some other authors prefer a different approach to power the inverters with field-oriented control (FOC)-based control and single-stage only with a single PV panel [21]. Other methods comprise neutral point clamped, flying-capacitor, or cascaded inverter circuits. Some recent research [22,23] is also very promising in delivering efficient utilization of sources. A similar objective is achieved with a single-stage different power circuit using a cascaded two-level inverter (CTLI) instead of a dc-dc intermediate converter presented in reference [18]. Moreover, the chosen CTLI can perform with less harmonic content in output, as suggested in the existing reference [24].

The control section of the circuits is comprised of various control strategies. Recently developed single-stage power circuit systems [25–27,30] can also deliver their promise.

In this work, a three-stage controller based on FOC has been chosen in combination with a progressive step perturb and observe (PSPnO) MPPT controller to adapt a stand-alone non-linear load. The sources of this system are two isolated low-

Department of Electrical Engineering, National Institute of Technology Durgapur, Durgapur, 713209, West Bengal, India
E-mails: sg.15ee1508@phd.nitdgp.ac.in, tapas.saha@ee.nitdgp.ac.in

voltage PV panels combined with a CTLI connected to the driving squirrel cage induction motor (SCIM) by an open-end primary, low-voltage (LV) side, and star-connected secondary, high-voltage (HV) side to avoid PSC condition.

The contribution of the work is:

i. The development of PSPnO MPPT control for CTLI-based PV system for the first time in the available literature.

ii. The PSPnO MPPT control has the advantage of shorter response time and smoother waveform over conventional fixed step PnO as presented in [28].

iii. The controlled system is successfully operated with a non-linear load under variable solar irradiance levels.

2. MODELING OF THE SYSTEM

2.1. PHOTOVOLTAIC CELL EQUIVALENT MODEL

A PV cell composed of a p-n junction resembles a diode consisting of a single p-n junction. But, as the PV cell generates varying currents depending on various conditions, its equivalent circuit must include a current source. In this article, a single equivalent circuit model of PV cells has been considered for the simulation environment. This model comprises a diode in parallel with a current source and a shunt resistor, and this is in series with another resistor; namely, series resistors are assumed as 323 Ω and 0.4 Ω, respectively. If such cells of X number are connected in series, forming a chain, and such chains of Y numbers are connected in parallel, the PV panel of our requirement is made. The current output of such a panel is derived from eq. 1. In our case, PV cells in series are taken ($Y = 12$). In such a string of PV cells in parallel ($X = 750$), a PV panel is formed and delivers maximum power in the 45 to 52 V range for normal Indian solar insolation.

$$I = X \left[I_{vcse} - I_{ser} \left[e^{\left(\frac{q\left(\frac{V}{Y} + \frac{I}{X} R_{ser}\right)}{n K_B T} \right)} - 1 \right] \right] - \left[\frac{V + R_{ser} I}{R_{shunt}} \right]. \quad (1)$$

2.2. PROPOSED SYSTEM'S POWER SCHEMATIC

The power circuit is described in Fig. 1. This power circuit comprises two isolated PV panels connected to each of the 3-phase inverters combined by an open-end winding 3-phase transformer's LV side, forming a CTLI. The transformer's HV side is connected in star formations and supplies power to a squirrel cage induction motor. The CTLIs are using 12 MOSFETs as switching devices. The space vector pulse width modulation (SVPWM) algorithm synchronizes and controls all those switches.

2.3. PROPORTIONAL STEP MPPT SCHEME

The MPPT algorithm generally tracks the maximum power extraction point from any non-linearly varying source. A source like the PV model governed by eq. 1 can only generate maximum power at a particular operating voltage for a given solar insolation and temperature. In such a system, an MPPT algorithm is very useful. The FSPnO MPPT algorithm is lightweight and can be implemented on a low computational power microcontroller. This FSPnO MPPT flowchart in Fig. 2 creates a perturbation in controller voltage output and observes machine response concerning power consumption.

It deviates the dc-bus voltage in the direction depending on the sign of power deviation versus voltage deviation gradient. However, this type of FSPnO MPPT has the limitation of being slow in response and oscillating in the final output voltage. To address this issue, a proportional step MPPT has been developed.

This MPPT flowchart, as in Fig. 3, has a progressive step response with the sign as previously discussed. Its voltage deviation output steps are also proportional to the power deviation magnitude. The flowchart also limits the step size to some extent so that the controller does not suffer from controllability issues. Thus, it eliminates the system's sluggish response time and oscillation issues.
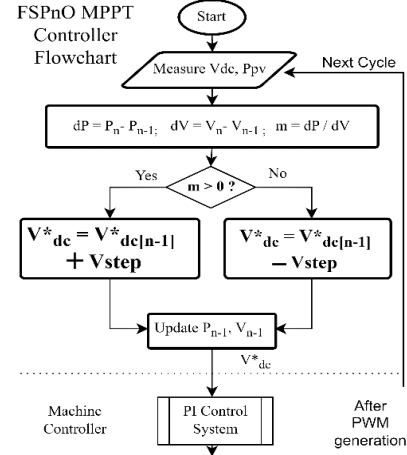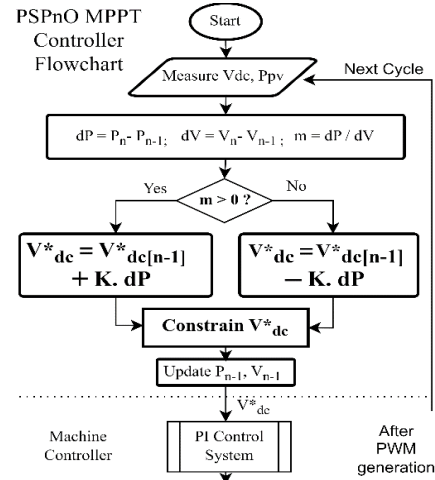

Fig. 2 – FSPnO MPPT.

Fig. 3 – PSPnO MPPT.

2.4. DESCRIPTION OF THE PROPOSED DRIVE'S CONTROL SYSTEM

The control topology of this system is focused mainly on maintaining dc-bus voltage at a given voltage determined by PSPnO MPPT, as discussed in the previous subsection. The controller governs the dc-bus by operating a SCIM to balance the power developed by PV panels. The block diagram in Fig. 4 and the mathematical equations below describe the operating principle of the control system.

The electromagnetic torque T_{em} developed in the induction motor can be defined by

$$T_{em} = \frac{2}{3} \frac{p}{2} \frac{L_m}{L_r} i_{QS} \Psi_r. \quad (2)$$

So, to control the torque in the SCIM and control the system through dc-link voltage control, we need speed reference generated by the voltage controller,

$$\omega^* = \left(k_{pv} + \frac{k_{iv}}{s} \right) \left(V_{DCL}^* - V_{DCL} \right). \quad (3)$$

The reference electromagnetic torque generated in the speed controller can be expressed by

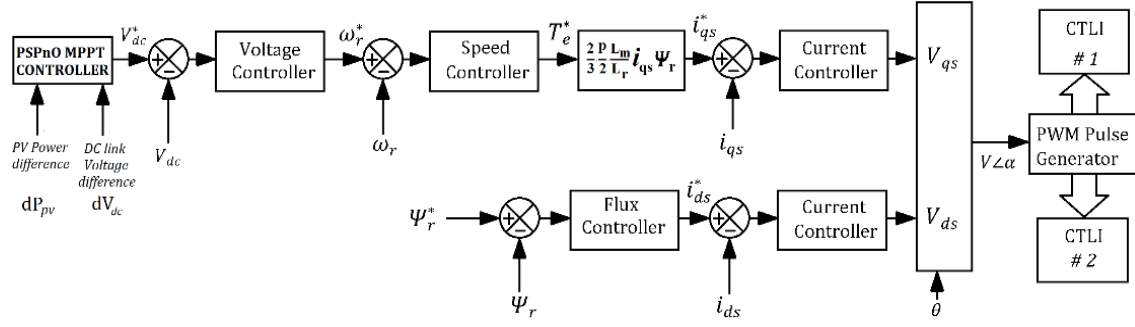$$T_{em}^* = \left(k_{ps} + \frac{k_{is}}{s} \right) \left(\omega^* - \omega_r \right). \quad (4)$$

Fig. 4 – Proposed control system block diagram.

The result of the previous step converges to the equation to generate $i*_{QS}$ in the current controller is,

$$i^*_{QS} = \left(k_{pc} + \frac{k_{ic}}{s}\right)\left(\Psi^*_r - \Psi_r\right). \qquad (5)$$

Thus, the expression of Q-axis voltage can be described by

$$V^r_{QS} = \left(R_s i^r_{QS} + \sigma L_s \frac{di^r_{QS}}{dt}\right) +$$
$$+ \frac{L_m}{L_r}\Psi_r(\omega_{mr} + \omega_e) + \sigma L_s i^r_{DS}(\omega_{mr} + \omega_e). \qquad (6)$$

Similarly, for the d-axis current, from flux reference $\Psi*_r$, the flux linkage controller generates $i*_{DS}$, which passes through the d-axis current controller, and, finally, we have an equation defining

$$V^r_{DS} = \left(R_s i^r_{DS} + \sigma L_s \frac{di^r_{DS}}{dt}\right) + \frac{L_m}{L_r}\frac{d\Psi_r}{dt} - \sigma L_s i^r_{QS}(\omega_{mr} + \omega_e). \qquad (7)$$

2.5. CONTROLLER DESIGN AND RESPONSES

Illustrated in Fig. 4, a cascaded configuration of three PI controllers is utilized. The foremost block in the outermost loop is the voltage controller, receiving input from the PSPnO MPPT controller. As designed, this block exhibits a corner frequency of 333 rad/s, depicted in Fig. 5. Subsequent block, a speed controller, transforms speed reference input into torque reference with a corner frequency of 1 000 rad/s, outlined in Fig. 6.
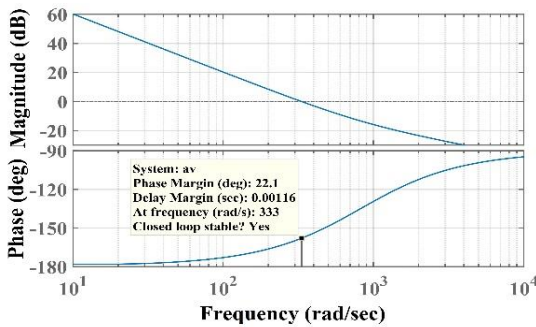

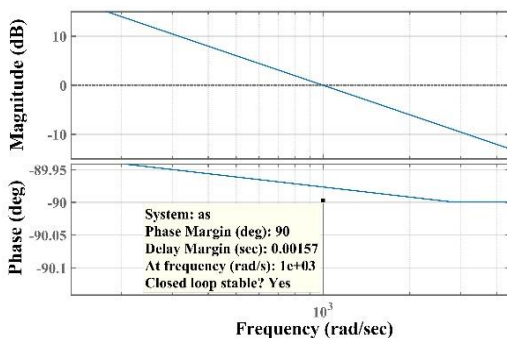Fig. 5 – Voltage controller bode plot.
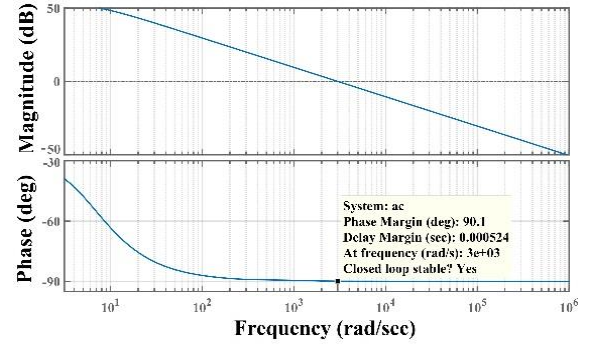

Fig. 6 – Speed controller bode plot.

Fig. 7 – Current controller bode plot.

In the innermost loop, the current controller utilizes torque reference input to generate the current reference for the corresponding axis. As shown in Fig. 7, this controller is designed with a 3 000 rad/s corner frequency, ensuring optimal current regulation.

3. SIMULATION

3.1. SYSTEM CONFIGURATIONS

The proposed control system of the mentioned scheme was simulated in a SIMULINK environment, maintaining the following hardware specifications and input conditions:

PV panel. Two panels, each with a capacity of 460 W peak for insolation at 1000 W/m^2.

CTLI. Two sets of 3-phase 2-level voltage source inverters are cascaded to form a CTLI, equipped with 12 MOSFETs, each rated at 100V, 28 A, and $R_{DS} = 0.4$ mΩ (in ON state).

Transformer. One 3-phase 5 kVA, 48/230 V transformer, LV side: open-end winding, HV side: star connected with neutral grounding.

Motor. One SCIM with a rating of 3-phase, 1.5 kW, 415 V, 50 Hz, 4 poles.

Nonlinear rotational load. The SCIM driving a load defined by $T_{load} = J_{load}\frac{d\omega}{dx} + F_{load}\omega + K_{load}\omega^2$ may resemble a centrifugal pump's theoretical torque-speed characteristics. Here, J_{load} = coefficient of rotational load's inertia, F_{load} = coefficient of friction and other load losses, and K_{load} = of non-linear load torque coefficient.

3.2. SIMULATION INPUTS

The study of the system was carried out based on the time frame as described, while the temperature is static at 27 °C.
- The PSPnO MPPT algorithm takes control of voltage reference generation at 4.5 s in both cases.

- Solar insolation increased from 800W/m² to 1 000W/m² at 10.0 s.
- From 10.0 s to 20.0 s it is constant at 1 000W/m².
- Solar insolation decreased from 1 000W/m² to 800W/m² at 20.0 s.

4. RESULT ANALYSIS

4.1. PSPNO MPPT'S DC-LINK VOLTAGE RESPONSE UNDER SOLAR INSOLATION DEVIATION

The total power developed curve in Fig. 8 results from steep dc-link voltage variation to shift the MPP. The first rise from 4.5 s to 5 s occurs from the control shift to the PSPnO MPPT algorithm, where it reaches the maximum power point (MPP) and stabilizes with minimal fluctuations. Another sharp rise and fall along with stable power due to variation in solar irradiance in the power curve is evident in the fact that the MPPT tracks and maintains the generated power at its MPP. Thus, the MPPT algorithm is very efficient and purposeful, subject to its application.
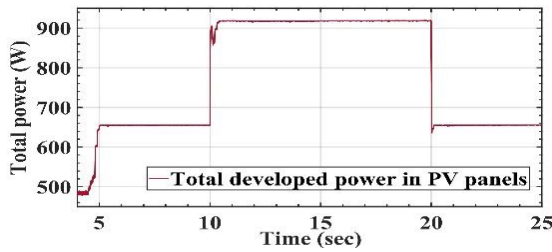
Fig. 8 – Total power developed in PV panel.

4.2. RESPONSE OF CONTROLLERS ON NON-LINEAR LOAD TORQUE

The variation in the solar irradiance test successfully proves the effectivity when a sudden change in solar insolation occurs. The MPPT quickly responds and increases the voltage step to a very high amount, considering the handling capability of the control system. This sudden high step resolves the MPPT voltage shift issue very quickly. As the difference between MPP voltage and dc-link voltage becomes minimal, the step size also reduces accordingly to a minimum value such that it can detect a further change and does not introduce ripples in the system performance. Figure 9a shows the system's response from the dc link voltage point of view. The governing equation of the load torque as seen by the motor, described in subsection 3.1, is similar to an ideal centrifugal pump's torque-speed characteristics. The first part of the equation describes the rotational inertia of the load, the next part represents the frictional and other losses that are proportional to the rotation, and the last part is for the load torque, which occurs by the non-linearity of the load and is proportional to the square of rotation. The change in irradiance on the PV panels results in a change in power generation, as described in the previous section. The rise and fall of power affect the rotation of the motor and, thus, results in a deviation of load torque T_{load}. The 3-stage PI controller plays a crucial role in maintaining the MPPT set voltage levels, as discussed in subsection 2.4 of this article. The control system adapts to any sudden alteration in the load torque and counters it by developing the required amount of torque by varying the q-axis current proportionally and speed inversely, keeping the power and voltage preserved at the same level defined by the MPPT algorithm. The outputs from the PI controllers are furnished as voltage controller in Fig. 9a, speed controller in Fig. 9b, and current controller in Fig. 9c. The load torque and developed torque are presented in Fig. 9d. As seen, the system accustomed to a new set-speed within 1 s of the input changes are made.
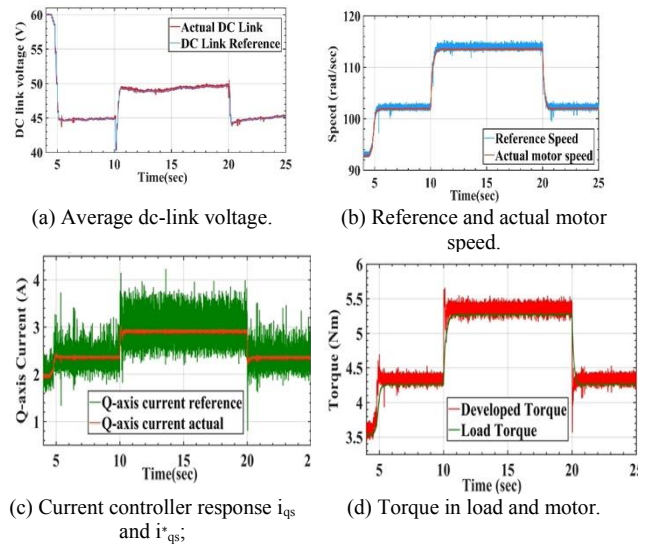
(a) Average dc-link voltage.

(b) Reference and actual motor speed.

(c) Current controller response i_{qs} and i^*_{qs};

(d) Torque in load and motor.

Fig. 9 – The responses of controllers under non-linear load.

4.3. COMPARISON BETWEEN PSPNO AND CONVENTIONAL FSPNO MPPT

While comparing with conventional FSPnO MPPT, in both MPPT algorithms, the period is taken as 100 ms. Starting with total PV power development, in the comparison simulations in Fig. 10, we see that the power development levels are the same for similar insolation. However, the PSPnO MPPT delivers power with lesser fluctuation throughout the simulation.
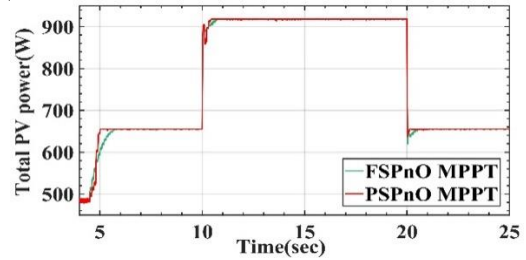
Fig. 10 – Total PV power generation comparison.

The dc-link voltage generated with both algorithms also proves that both algorithms track near MPP, but the PSPnO MPPT produces far stable voltage levels for given insolation. This results in stable power delivery to the system under simulation. Table 1 is vibrant enough to evidence this. Also, it is to be noted that the PSPnO MPPT is faster in tracking in case of insolation change or while starting (Fig. 11).
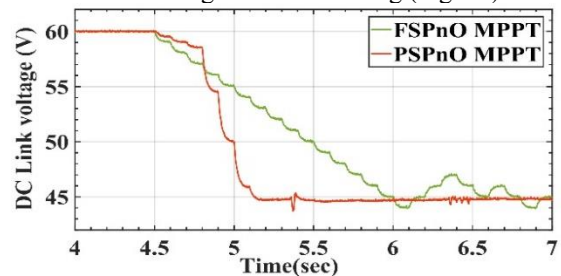
Fig. 11 – Close-up view of dc-link (4.0 s to 7.0 s) at starting.

Table 1 also demonstrates that at time 4.5 s, both MPPT algorithms are taking necessary tracking action towards MPP. However, the PSPnO MPPT is swifter in achieving the optimum voltage level and preserving it efficiently within an envelope of 0.2 V. In contrast, the FSPnO MPPT is not only slower by 0.825 s but also maintains an envelope of 1.0 V as per its algorithm. This PSPnO MPPT responds faster, resulting in more energy harvesting from PV panels with frequent alteration in insolation input. Thus, it is more energy-cost efficient than FSPnO.

Table 1

Dc-link voltage comparison for PSPnO and FSPnO MPPT

Time (Sec)	Dc-link voltage (V)	
	PSPnO MPPT	FSPnO MPPT
2.00	60.00	60.00
2.50	60.00	60.00
3.00	60.00	60.00
3.50	60.00	60.00
4.00	60.00	60.00
4.50	60.00	60.00
5.00	50.20	55.10
5.50	44.70	50.20
6.00	44.70	45.10
6.50	44.80	46.00
7.00	44.70	45.00
7.50	44.60	44.00
8.00	44.90	45.00
8.50	44.90	46.00
9.00	44.70	47.00
9.50	45.10	46.00
10.00	44.90	45.00
10.50	49.00	45.70
11.00	49.20	51.00
11.50	49.10	50.10
12.00	49.00	51.00
12.50	48.80	50.00
13.00	49.10	49.10
13.50	48.70	50.00
14.00	49.00	51.00
14.50	48.90	50.00
15.00	49.10	49.00
15.50	49.30	49.90
16.00	49.40	51.00
16.50	49.30	50.00
17.00	49.30	49.10
17.50	49.50	50.00
18.00	49.60	51.20
18.50	49.60	50.00
19.00	49.50	49.00
19.50	49.70	50.20
20.00	49.80	51.10
20.50	44.30	48.10
21.00	44.40	47.00
21.50	44.70	46.00
22.00	44.90	45.00
22.50	44.80	46.00
23.00	44.90	45.00
23.50	45.00	46.10
24.00	45.10	45.00
24.50	45.10	46.00
25.00	45.30	45.00

Figure 12a reveals that the PSPnO MPPT algorithm successfully tracks the reference speed in less time than the FSPnO MPPT. Comparing the time aspect, it is seen that the PSPnO MPPT responds with faster output than the previous cases, and the speed curve oscillations are also greatly reduced while using this MPPT algorithm, as illustrated in Fig. 12(b). Its inherent property significantly reduces motor speed oscillation and thus increases the life expectancy of mechanical structure integrity and noise of the used motor.
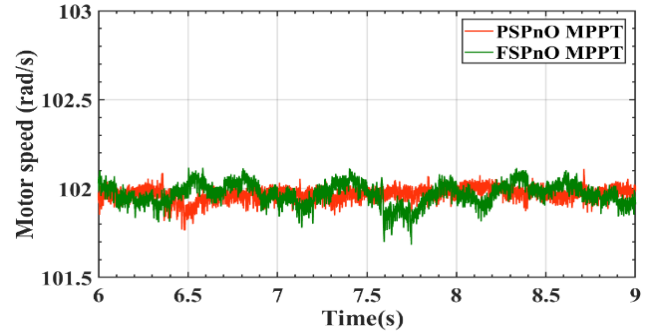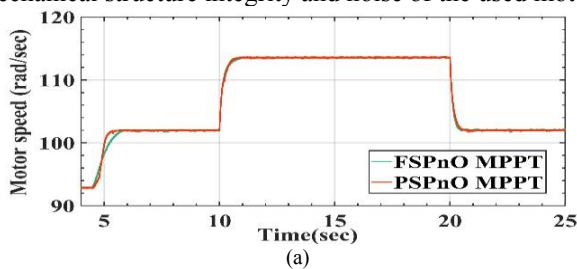
(b)

Fig. 12 – Motor speed comparison of PSPnO MPPT and FSPnO :
a) complete curve; b) zoom of complete curve's 6.0s to 9.0 s.

5. CONCLUSION

The result and discussion show that the proposed PSPnO MPPT algorithm can track and maintain its CTLI's dc-link voltages near MPP even under unpredictable changes in solar insolation. The developed power depends only on the variation of solar insolation level and not on load torque. The developed power, DC link voltage, and motor speed tracking are faster than FSPnO MPPT. The curves mentioned in the above points are also smoother compared to prior cases of conventional FSPnO MPPT. The 3-stage control system for SCIM can handle non-linear load torque. The CTLI's based on SVPWM generated a 7-level voltage at the output stage. Based on the analysis, this work has successfully developed a PSPnO MPPT, which, along with its 3-stage PI control system and SVPWM-based CTLI power circuit, can outperform conventional FSPnO MPPT while running on very low computational overhead. Hardware validation of the proposed scheme contributed to the future scope of this work.

NOMENCLATURE

V = PV cell terminal voltage.
I = PV cell terminal current.
I_{vcse} = photo-generated current (linear with irradiance).
I_{ser} = Saturation current due to diffusion mechanism.
q = charge of electron [$1.6 \times 10^{(-19)}$ C].
R_{ser} = PV cell series resistance [Ω].
R_{shunt} = PV cell shunt resistance [Ω].
n = diode quality factor [$n = 2$ for silicon diode].
K_B = Boltzmann's constant [$1.38 \times 10^{(-23)}$ J/K].
T = Temperature of PV cells in Kelvin.
X = Number of PV cells connected in series.
Y = Number of series cells connected in parallel.
V_{step} = Step voltage of FSPnO MPPT.
K = Progressive step gain.
V_{QS}^r, V_{DS}^r = Voltage output of 'q' and 'd' axis controllers.
i_{QS}, i_{QS}^* = Q-axis stator current and its reference value.
i_{QS}^r, i_{DS}^r = stator 'q' & 'd'-axis currents in rotor reference frame.
V_{DCL}, V_{DCL}^r = dc-link voltage and its reference.
T_{em} = Electromagnetic torque [Nm].
L_r, L_s, L_m = Rotor, stator, and mutual inductances.
R_r, R_s = Rotor and stator resistances.
$K_{pv}, K_{iv}, K_{ps}, K_{is}, K_{pc}, K_{ic}$ = Proportional [p] & integral [i] gains of voltage[v], speed[s] & current[c] controllers.
$\omega_r, \omega_{mr}, \omega_e, \omega^*$ = Rotor, slip, electrical rotational speeds, and rotor speed reference.
Ψ_r, Ψ_r^* = Rotor flux linkage and its reference.
$\sigma = 1 - \frac{L_m^2}{L_r L_s}$.

(a)

REFERENCES

1. G. Yadav, K.K. Jaladi, *Comparison of different parameters using single diode and double diode model of PV module in a PV-battery system using Matlab Simulink*, 2017 14th IEEE India Council International Conference (INDICON), India (15–17 December 2017).

2. A.M. Humada, M. Hojabri, S. Mekhilef, H.M. Hamada, *Solar cell parameters extraction based on single and double-diode models: A review*, Renewable and Sustainable Energy Reviews, **56**, pp. 494–509 (2016).

3. S. Pindado, J. Cubas, *Simple mathematical approach to solar cell/panel behavior based on datasheet information*, Renewable Energy, **103**, pp. 729–738 (2017).

4. S. Saravanan, N. Ramesh Babu, *Maximum power point tracking algorithms for photovoltaic system a review*, Renewable and Sustainable Energy Reviews, **57**, pp. 192–204 (2016).

5. D. Kumar, K. Chatterjee, *A review of conventional and advanced MPPT algorithms for wind energy systems*, Renewable and Sustainable Energy Reviews, **55**, pp. 957–970 (2016).

6. M. Garbarino, R. Morales, P. Henriquez, S. Cuevas, J. Rohten, A. Rubio, E. Wernekinck, P. Melin, *Comparison between maximum power point tracking algorithms for dc/dc power converters*, Chilean Conference on Electrical, Electronics Engineering, Information and Communication Technologies (CHILECON), Chile (18–20 October 2017).

7. S.N. Figueiredo, R.N.A.L.S. Aquino, M.E.P.V. Zurita, *Comparison between p&o-based and PSO-based MPPT algorithms for photovoltaic system under partially shaded conditions*, 6th International Conference on Control, Decision and Information Technologies (CoDIT), Paris, France (23–26 April 2019).

8. A.K. Soni, K.C. Jana, D.K. Gupta: Variable step-size adaptive maximum power point tracking algorithm for solar cell under partial shading conditions, IETE Journal of Research, **69**, *3*, pp. 1562–1577 (2021).

9. H.H.H. Mousa, A.-R. Youssef, E.E.M. Mohamed, *Variable step size P&O MPPT algorithm for optimal power extraction of multi-phase PMSG based wind generation system*, International Journal of Electrical Power & Energy Systems, **108**, pp. 218–231 (2019).

10. E.K. Anto, J.A. Asumadu, P.Y. Okyere, *PID control for improving P&O MPPT performance of a grid-connected solar PV system with Ziegler-Nichols tuning method*, IEEE 11th Conference on Industrial Electronics and Applications (ICIEA), Hefei, China (05–07 June 2016).

11. D. Jiandong, X. Ma, S. Tuo, *A variable step size P&O MPPT algorithm for three-phase grid-connected PV systems*, China International Conference on Electricity Distribution (CICED), Tianjin, China (17–19 September 2018).

12. A.A. Kulaksiz, R. Akkaya, *A genetic algorithm optimized ANN-based MPPT algorithm for a stand-alone PV system with induction motor drive*, Solar Energy, **86**, *9*, pp. 2366–2375 (2012).

13. A. Harrag, S. Messalti, *Variable step size modified P&O MPPT algorithm using ga-based hybrid offline/online PID controller*, Renewable and Sustainable Energy Reviews, **49**, pp. 1247–1260 (2015).

14. H.K. Varma Gadiraju, V. Reddy Barry, I. Maraka, *Dynamic photovoltaic array reconfiguration for standalone PV water pumping system*, 8th International Conference on Power Systems (ICPS), Jaipur, India (20–22 December 2019).

15. H.K.V. Gadiraju, B.V. Reddy, R.K. Jain, *Reconfiguration based single stage PV water pumping system*, National Power Electronics Conference (NPEC), Tiruchirappalli, India (13–15 December 2019).

16. A.K. Ranjan, A. Yadav, N. Pal, *Application of cascaded H-bridge multi-level inverter for PV based induction motor*, 3rd International Conference on Recent Developments in Control, Automation & Power Engineering (RDCAPE), Noida, India (10–11 October 2019).

17. N. Yussif, A.S. Abdel-Khalik, A.M. Mohamed, *An improved quadratic V/f-based control of photovoltaic battery-less induction motor-driven water pumping system*, International Conference on Sustainable Energy Engineering and Application (ICSEEA), Tangerang, Indonesia (23–24 October 2019).

18. Z. Massaq, A. Abounada, G. Chbirik, M. Ramzi, A. Brahmi, *Double stage solar PV array fed sensorless vector-controlled induction motor for irrigational purpose*, 7th International Renewable and Sustainable Energy Conference (IRSEC), Agadir, Morocco (27–30 November 2019).

19. R. Saxena, S.K. Sharma, M. Dubey, *Sepic converter based solar energy driven sensorless induction motor drive*, IEEE International Conference on Power Electronics, Smart Grid and Renewable Energy (PESGRE2020), Cochin, India (02–04 January 2020).

20. A. Hadj Dida, M. Bourahla, H.B. Ertan, *Highly efficient multi-junction solar cells performance improvement for ac induction motor control using the dspic30f microcontroller*, International Aegean Conference on Electrical Machines and Power Electronics (ACEMP) & International Conference on Optimization of Electrical and Electronic Equipment (OPTIM), Istanbul, Turkey (27–29 August 2019).

21. R. Rai, S. Shukla, B. Singh, *Reactive power based MRAS for speed estimation of solar fed induction motor with improved feedback linearization for water pumping*, IEEE Transactions on Industrial Informatics, **16**, *7*, pp. 4714–4725 (2020).

22. A. Hota, M. Qasim, J.L. Kirtley, V. Agarwal, *Novel boost inverter configuration and $3 - \phi$ induction motor drive for home appliances*, Innovations in Power and Advanced Computing Technologies (i-PACT), Vellore, India (22–23 March 2019).

23. R. Rai, S. Shukla, B. Singh, *Sensorless field oriented SMCC based integral sliding mode for solar PV based induction motor drive for water pumping*, IEEE Transactions on Industry Applications, **56**, *5*, pp. 5056–5064 (2020).

24. N. Kumar, T. K. Saha, J. Dey, *Cascaded two-level inverter based grid-connected photovoltaic system: Modelling and control*, IEEE International Conference on Industrial Technology (ICIT), Busan, Korea (South) (26 February 2014 – 01 March 2014).

25. S. Ghosh and T. K. Saha, *Development and performance analysis of stand-alone PV-based induction motor drive*, Advances in Communication, Devices, and Networking, Lecture Notes in Electrical Engineering, Springer, Singapore, 2018, pp. 747–754.

26. R. Mishra, T. K. Saha, *Development of a standalone VSCF generation scheme through three-stage control of SCIG*, IEEE Region 10 Conference (TENCON), Singapore (22–25 November 2016).

27. R. Mishra and T. K. Saha, *Combined control of stand-alone energy conversion scheme for distributed sources: Development and performance analysis*, International Journal of Electrical Power & Energy Systems, **115**, Article 105480 (2020).

28. S. Ghosh, T. K. Saha, *Development and analysis of standalone PV MPPT driven induction motor drive*, International Journal of Mechanical and Production Engineering Research and Development (IJMPERD), Special Issue, pp. 241–247 (June 2018).

29. S. Seba, M. Birane, K. Benmouiza, *A comparative analysis of boost converter topologies for photovoltaic systems using MPPT (P&O) and beta methods under partial shading*, Rev. Roum. Sci. Techn. – Électrotechn. et Énerg., **68**, *4*, pp. 375–380 (2023).

30. E. Benyoussef, S. Barkat, *Direct torque control based on space vector modulation with balancing strategy of dual star induction motor*, Rev. Roum. Sci. Techn. – Électrotechn. et Énerg., **67**, *1*, pp. 15–20 (2022).